IJE TRANSACTIONS A: Basics Vol. 39, No. 10, (October 2026) 2361-2370

International Journal of Engineering

Journal Homepage: www.ije.ir

Microstructural and Mechanical Characteristics of AlCoCrFeNi-YSZ High Entropy Alloy Matrix Composite

M. Askarzadeh Ardestani[a], M. Farvizi*[b], A. Alizadeh Samiyan[a], M. Ghanbariha[a], T. Ebadzadeh[a], M. M. Kalantarian[a]

[a] *Department of Ceramic, Materials and Energy Research Center, Karaj, Iran*
[b] *Department of Materials Engineering, University of Tabriz, Tabriz, Iran*

PAPER INFO

Paper history:
Received 02 September 2025
Received in revised form 05 October 2025
Accepted 25 October 2025

Keywords:
High Entropy Alloy
Ceramic Particulates
Composite Materials
Mechanical Properties

ABSTRACT

In this study, high-entropy alloy matrix composites (HEAMCs) consisting of an AlCoCrFeNi matrix reinforced with zirconia-based particles were fabricated using mechanical alloying (MA) followed by spark plasma sintering (SPS). Microstructural analysis revealed the presence of both FCC and BCC phases after 30 hours of mechanical alloying and subsequent sintering at 1000 °C. Rietveld refinement analysis indicated that the weight fraction of the FCC phase remained nearly constant in both the HEA and HEA–YSZ composites. However, the addition of YSZ particles decreased the BCC phase content and restricted grain growth during sintering. Compressive test results showed that the specimen containing 5 wt.% YSZ exhibited the highest yield strength (1760 MPa), attributed to its higher BCC phase fraction (40%). In contrast, the specimen with 10 wt.% YSZ demonstrated reduced yield strength due to a lower BCC phase content (36%). These findings indicate that AlCoCrFeNi composites reinforced with YSZ possess higher yield strength than those reinforced with ZrO_2 when comparable reinforcement levels are used. This improvement is attributed to the higher BCC phase content and the superior intrinsic properties of YSZ. Fracture surface analysis confirmed the coexistence of both ductile and brittle fracture modes in the tested specimens.

doi: *10.5829/ije.2026.39.10a.01*

Graphical Abstract

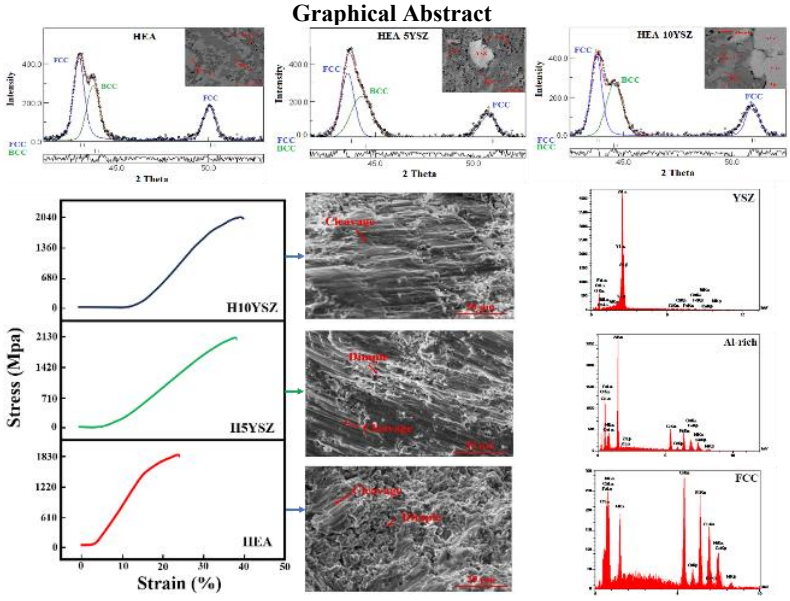

*Corresponding Author Email: *mmfarvizi@yahoo.com* (M. Farvizi)

Please cite this article as: Askarzadeh Ardestani M, Farvizi M, Alizadeh Samiyan A, Ghanbariha M, Ebadzadeh T, Kalantarian MM. Microstructural and Mechanical Characteristics of AlCoCrFeNi-YSZ High Entropy Alloy Matrix Composite. International Journal of Engineering, Transactions A: Basics. 2026;39(10):2361-70.

1. INTRODUCTION

As science and technology advance in material engineering, the alloying industry has undergone major changes. A notable advancement in materials science is the identification of new types of alloys known as high entropy alloys (HEAs) in 2004 (1-4). These alloys can be produced by mixing a minimum of five elements, ensuring their atomic percentages are equal to or nearly the same as one another (5-8). This has led to a high entropy effect in these alloys (4). The constituent elements' types and quantities are the primary factors influencing the microstructure and characteristics of high entropy alloys (6). HEAs can possess interesting properties, including high resistance to softening at elevated temperatures, low diffusion kinetics, high fracture and creep resistance, and good compressive strength at room temperature (7). HEAs mostly have a high melting point and maintain strength at extremely high temperatures (9).

The AlCoCrFeNi system has been extensively studied among various HEAs because of its remarkable characteristics (10-18). AlCoCrFeNi compounds can be used as the matrix of metal matrix composites (MMCs) because of their high specific strength compared to nickel- and titanium-based alloys and polymers (7). AlxCoCrFeNi HEAs are relatively lightweight and exhibit high compressive strength and excellent structural flexibility, particularly when compared to other HEAs such as CoCrFeNiMn and refractory HEAs (19-26).

Recent studies have indicated that optimizing material composition, processing parameters, and microstructural design can significantly enhance the tribological behavior, wear resistance, and energy absorption capacity of advanced composite systems used in dynamic and high-friction environments (27-30). Incorporating hard ceramic particles into MMCs is an effective method to enhance mechanical properties such as wear resistance, hardness, compressive strength, and toughness compared to the base metal (31).

Zirconia is an interesting material for various applications due to its notable characteristics, including a high elastic modulus, outstanding hardness, and elevated melting point (32, 33). Earlier studies have demonstrated that incorporating ZrO_2 into alloys such as Al, Cu, and Mg can enhance both the mechanical and tribological characteristics of these materials (34-36). However, at 1100°C, a phase transformation occurs between the monoclinic and tetragonal phases of zirconia, accompanied by a considerable volume change that can negatively affect the properties of this phase (37). Therefore, different oxides such as Y_2O_3 can be added to ZrO_2 to restrict this transformation. The addition of yttrium oxide stabilizes the tetragonal phase of zirconia at high temperatures and prevents transformation to the stable monoclinic phase at room temperature (37). Previous investigations have demonstrated that YSZ possesses superior mechanical properties compared with ZrO_2. Specifically, YSZ exhibits higher elastic modulus, hardness, and compressive strength than zirconia. Moreover, its higher coefficient of thermal expansion (CTE) relative to monoclinic zirconia helps to minimize thermal mismatch stresses during the sintering process (38).

There are only limited studies on HEA matrix composites reinforced with ceramic particles. In research by Ghanbariha et al. (39), AlCoCrFeNi reinforced with monoclinic zirconia particles was produced by the MA-SPS technique, and the effect of these particles on the microstructural aspects of AlCoCrFeNi-ZrO_2 composites was studied. According to their results, all specimens after the SPS process had two main phases, including FCC and BCC. It was also found that zirconia particles had a positive impact on the wear resistance of HEA-ZrO_2 composites (40).

Due to the superior properties of YSZ compared to ZrO_2 in metal matrix composites, this study focuses on producing AlCoCrFeNi-YSZ composites using the MA-SPS method. The microstructural characteristics and mechanical properties of these composites are systematically investigated and compared with AlCoCrFeNi-ZrO_2 composites. The primary objective of this research is to evaluate the effectiveness of YSZ reinforcement in enhancing the mechanical performance of AlCoCrFeNi-based HEA composites and to provide insights for the development of high-performance HEA matrix composites.

2. MATERIALS AND METHODS

Figure 1 presents the XRD and SEM images of the initial YSZ powder. The specimens were fabricated through mechanical alloying combined with the spark plasma sintering method. The details of this procedure were discussed by Ghanbariha et al. (39) and depicted in

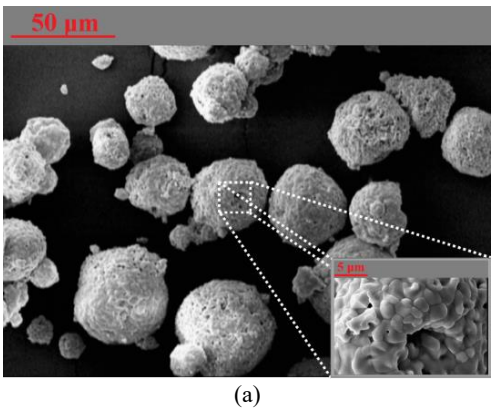

(a)

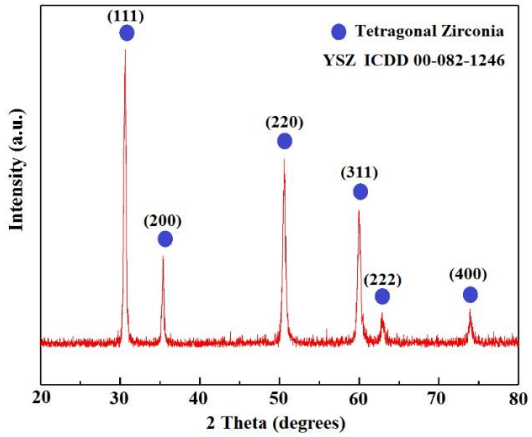

(b)

Figure 1. (a) SEM image, and (b) XRD pattern of YSZ powder

Figure 2. The identification of the phases in the raw powders and the sintered specimens was performed using X-ray diffraction (XRD - CuK_α radiation: at 20 kV, λ = 0.154 nm, and 30 mA) (D-500, Siemens, Germany). Each diffraction pattern was recorded with a step size of 0.2. For the analysis of microstructure, field emission scanning electron microscopy (FESEM, TESCAN MIRA3, Czech Republic) was used in conjunction with energy dispersive spectroscopy (EDS). Material analysis utilizing diffraction (MAUD) software was employed to acquire crystallographic data on the relevant phases, along with quantitative analysis of the specimens through the Rietveld refinement method. During all Rietveld refinement procedures, the R and sigma values were consistently below 10 and 2, respectively.

Compression tests were performed according to E3 standard with a 1 mm/min shear rate at room temperature. For this purpose, cylindrical specimens were prepared with a thickness and diameter of 5.2 mm by an electrical discharge machine (EDM). Every experiment was conducted three times to confirm the reliability of the results.

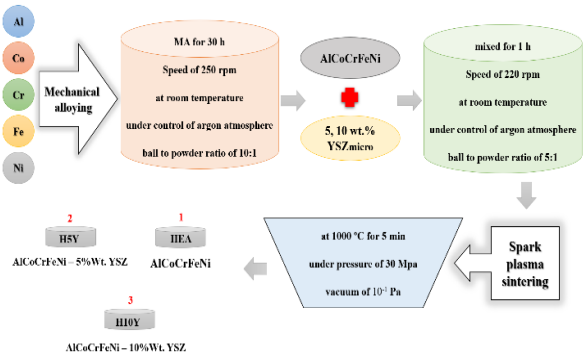

Figure 2. Details of MA and SPS process

3. RESULT AND DISCUSSION

3. 1. Synthesis of HEA Powder Figure 3 displays the SEM micrograph of the HEA powder produced using MA. This image shows that the spherical powders are formed by the cold-welding process during MA. The difference in the inherent hardness of the initial powders activated two main mechanisms — fracture and cold welding (brittle–soft and soft–soft) — that contributed to quasi-spherical particle formation and uniform powder mixing. During the process, due to the increase in temperature, diffusion of atoms within the crystal lattice of other atoms and self-diffusion are activated. The evolved BCC phase results from crushing due to work hardening of the powders and an increase in dislocation density, which enhances diffusion pathways. The particle size reduction and simultaneous diffusion continue until the alloy system appears as a single powder.

3. 2. SPS of AlCoCrFeNi-YSZ (micro) HEA To gain insights into how YSZ reinforcement influences the phase components and the proportion of phases within HEA matrix composites, Rietveld refinement analysis was employed. The regions extracted from Rietveld refinement analysis are shown in Figure 4(a-c). Figure 4 illustrates scans for the (111) plane of the FCC phase as well as the (110) plane of the BCC phase for the HEA, H5Y, and H10Y specimens. The outcomes from this analysis are summarized in Table 1. Prior to SPS, the HEA powder had a crystallite size of approximately 5 nm, while following the SPS process, the crystallite size for the BCC phase of the HEA specimen increased to 80 nm and for the FCC phase to about 38 nm. Notably, when 10 wt.% YSZ was incorporated, the crystallite sizes of the FCC and BCC phases became approximately 29 nm and 79 nm, respectively, indicating that these particles hinder grain growth in the HEA matrix. In general, secondary particles in the matrix, whether formed in situ

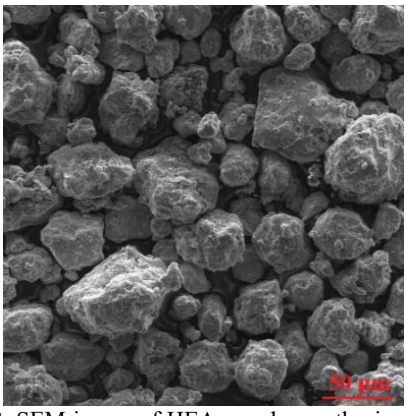

Figure 3. SEM image of HEA powder synthesized by MA after 30 hours

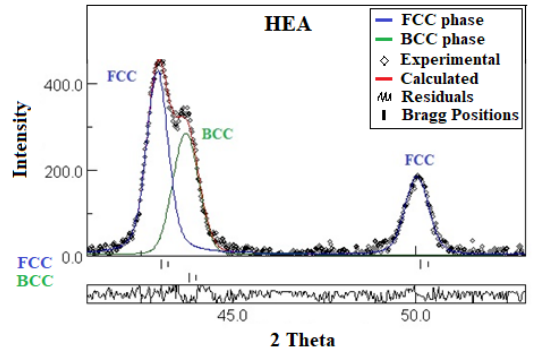

(a)

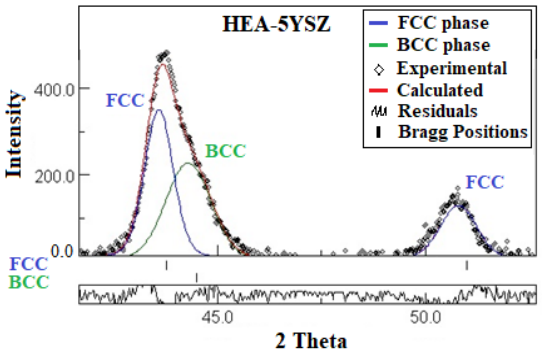

(b)

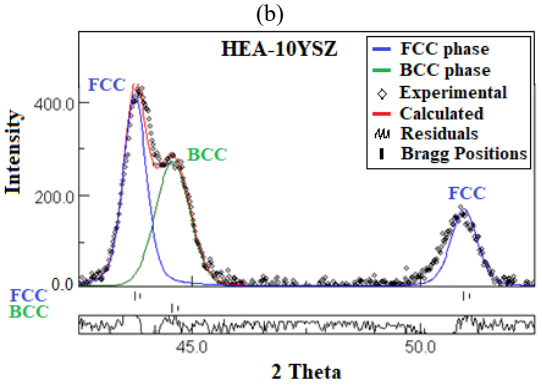

(c)

Figure 4. (a, b, c) Result Rietveld refinement with the detailed scans for FCC and BCC phases of all specimens

or added externally, prevent grain growth through pinning (41). In the AlCoCrFeNi-ZrO_2 specimen, incorporating 10 wt.% zirconia resulted in crystallite sizes of the FCC and BCC phases to reach 21 nm and 78 nm, respectively (39). This suggests ZrO_2 particles are more effective at inhibiting grain growth than YSZ particles. The relatively higher diffusion coefficient of YSZ particles, due to oxygen vacancies, facilitates grain growth. Consequently, ZrO_2 exhibits a stronger capacity to prevent grain growth. Additionally, zirconia particles, owing to their irregular shape, provide a larger surface area for nucleation compared to spherical YSZ particles.

The data shown in Table 1 indicates that the weight percentage of the FCC phase in HEA and HEA composites remains relatively stable as the YSZ content increases during the SPS process; however, the BCC phase content diminishes in the composites. The reduction in BCC phase with increasing reinforcement particles can be attributed to the formation of interfaces and dislocations, which cause active elements such as aluminum to be extracted from the BCC phase—known for its higher aluminum content—and relocate to the interface between HEA and YSZ particles, resulting in the formation of an Al-rich phase. This explanation aligns with the findings presented in Table 1 and Figures 6 and 7.

3. 3. Microstructural Evaluation Figure 5 shows the FESEM results with EDS analysis of AlCoCrFeNi after the SPS process. It is noted that the HEA consists of four primary phases: BCC (dark grey), FCC (bright), Cr-rich (gray), and Al-rich (black) phases. According to the EDS data shown in Table 2, the BCC phase exhibits a high weight percentage of Al and Ni, while displaying lower weight percentages of Cr, Fe, and Co. Conversely, the FCC phase has a greater concentration of Cr, Fe, and Co, with a reduced presence of Al and Ni. Furthermore, the microstructure of this specimen displays small black dots, identified as Al-rich phases.

Figure 6 shows FESEM images of AlCoCrFeNi-5wt.% YSZ following the sintering process. In this specimen, in addition to the YSZ reinforcement particles that are visible as white within the HEA matrix, three other phases (FCC, BCC, and Al-rich) have been recognized. The FCC phase is characterized by a high concentration of Fe, Cr, and Co, whereas the BCC phase is predominantly composed of Al and Ni. According to

TABLE 1. Structural data of HEA-YSZ (micro) composites obtained from Rietveld refinement

YSZ (wt.%)	**0** (39)		**5**		**10**	
Crystal system	FCC	BCC	FCC	BCC	FCC	BCC
Space group	Fm-3m	Im-3m	Fm-3m	Im-3m	Fm-3m	Im-3m
Unit cell	0.36	0.28	0.35	0.28	0.35	0.28
Crystallite size (nm)	38.21	80.04	27.17	79.03	29.89	79.84
Phase fraction (wt. %)	55.85	44.15	54.80	40.20	54.00	36.00

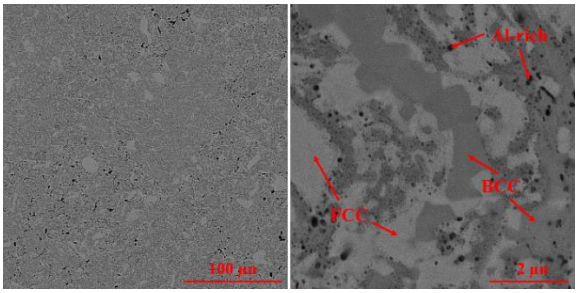

(a)

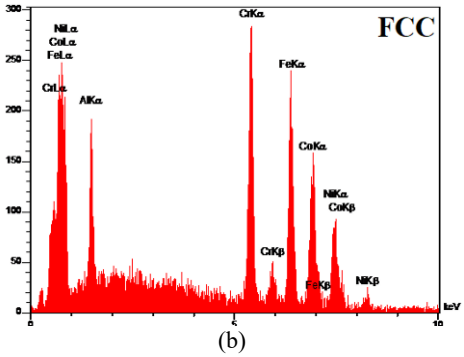

(b)

Figure 5. a) SEM image of the SPS-processed AlCoCrFeNi, and b) EDS analysis

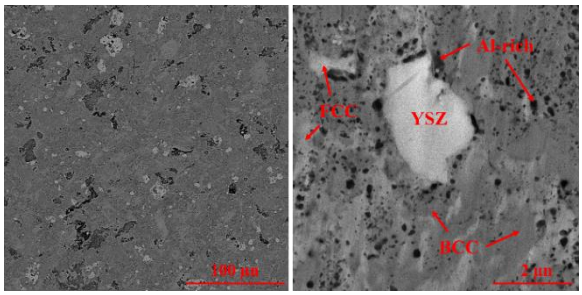

(a)

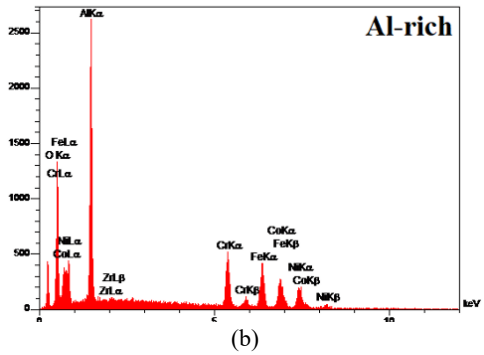

(b)

Figure 6. a) SEM image of the SPS-processed AlCoCrFeNi-5 wt. % YSZ, and b) EDS analysis

prior research (39), a comparison of HEA-5 wt.% ZrO_2 and HEA-5 wt.% YSZ showed that the amounts of Al and Co in the FCC phase of HEA-5 wt.% YSZ were significantly decreased to 3.72 and 23.69 wt.%, respectively, while the concentrations of these elements in the HEA-5 wt.% ZrO_2 specimen stayed relatively stable. Furthermore, there was a reduction in the weight percentage of Al in the BCC phase from 19.81 to 15.48 wt.%, whereas the data in Table 2 indicates that in the HEA-5 wt.% ZrO_2 specimen, this value increased to 20.77 wt.%. It is widely recognized that YSZ has a higher CTE than ZrO_2 and is more in line with the CTE of metals and alloys. As a result, the difference in thermal expansion coefficients between the matrix and reinforcement in the HEA-YSZ composite is less pronounced than that in the HEA-ZrO_2 composite. In the HEA-ZrO_2 composite specimen, it was observed that by adding zirconia reinforcement particles, the interface was created between the matrix and reinforcement, and the diffusion system was activated. As a result, active elements such as aluminum moved to the interface and an accumulation of Al-rich phase was created at the interface between HEA and ZrO_2 particles. However, in HEA-YSZ composite, due to the smaller difference in coefficient of expansion, the diffusion system is less activated and the rate of Al leaving the BCC phase and accumulating at the interface between HEA phase and YSZ particles will be less. According to these results, HEA-YSZ composite has more BCC phase and less Al-rich phase than HEA-ZrO_2 composite.

Figure 7 illustrates the FESEM micrographs of AlCoCrFeNi-10 wt.% YSZ after undergoing the SPS process. Similar to the earlier specimen, as indicated in Table 2, the predominant phase in the microstructure is the FCC phase, which is rich in Fe, Cr, and Co. Furthermore, the specimen also displayed the existence of BCC, Cr-rich, and Al-rich phases. The formation of the Al-rich phase is likely due to its higher diffusion coefficient. It is proposed that the relatively elevated diffusion coefficient of aluminum, in comparison to the other elements in the HEA system, may promote the development of this Al-rich phase (42). As it was revealed in previous study (35), in FCC phase of HEA-10 wt.% ZrO_2 specimen the amount of Co has decreased from 33.07 to 25.23 wt.%, in comparison with FCC phase of HEA-10 wt.% YSZ. In addition, in BCC phase related to HEA-10 wt.% YSZ, the amount of Ni and Al compared with HEA-10 wt.% ZrO_2 has decreased from 22.07 and 13.28 to 32.68 and 19.95 wt.%, respectively.

3. 4. Compressive Behavior To understand the influence of YSZ and monoclinic ZrO_2 particle addition on the compressive behavior of AlCoCrFeNi HEA matrix composites, compression tests were performed on the HEA-x wt.% YSZ and HEA-x wt.% ZrO_2 specimens. The related stress-strain curves are shown in Figures 8(a) and 8(b), respectively. The quantitative data obtained from these tests, including ε_p, σ_y, and σ_{max}, are

summarized in Table 3. The results of the compression tests indicate that the addition of ceramic particulates enhances the strength of the HEA matrix. This improvement is more pronounced in specimens with 5 wt.% reinforcement. According to Table 1, while the FCC phase fraction remains relatively unchanged, the addition of reinforcements leads to a reduction in the BCC phase content. There is a trade-off between ceramic reinforcement and BCC content. In the H5Y specimen, the yield strength increased to 1760 MPa. In contrast, the H10Y specimen exhibited a decrease in yield strength, attributed to a lower percentage of the BCC phase (36 wt.%). Similarly, the H5Z specimen, with 39% wt. BCC phase, achieved a yield strength of 1650 MPa, while the H10Z specimen, with a reduced BCC phase percentage (31 wt.%), exhibited a lower yield strength of 1550 MPa.

The characteristics of HEAs can differ significantly from those of their constituent elements. The structure type plays a crucial role in influencing the strength and hardness of HEAs. Generally, HEAs with a BCC structure demonstrate high yield strength but limited plasticity, whereas those with an FCC structure tend to have lower yield strength but greater ductility (5, 12, 13). Therefore, high yield strength (σ_y) is associated with the presence of the BCC structure, while ductility is attributed to the FCC structure (43).

Among the different kinds of engineering ceramics, zirconia and YSZ display notable mechanical characteristics like elevated hardness and elastic modulus, as well as significant wear resistance, which contributes to their effective use as reinforcing agents in various MMCs like NiTi (44), Cu (45), Ni-P (46), and Mg (47) composites. Also, inherently YSZ shows better physical and mechanical properties compared to monoclinic zirconia (45) which yields better mechanical properties of HEA-YSZ composites.

Zhou et al. (41) reported a yield strength of 1390 MPa for the AlCoCrFeNi alloy, which is lower than the yield strength (σ_y) reported in this study. In polycrystalline materials, the yield strength is influenced by multiple strengthening mechanisms, including grain boundary, precipitation, dislocation, thermal mismatch, and solid solution strengthening (47). In HEA matrix composites, the enhancement in strength is primarily due to the second phase strengthening resulting from the incorporation of monoclinic and YSZ particles, alongside thermal mismatch strengthening, which increases the density of dislocations and makes their movement more difficult, thereby reinforcing the matrix. Additional contributors to the improved compressive strength and yield strength may be linked to the characteristics of the employed synthesis method (MA+SPS) that can bolster material strength by refining the grain structure and introducing a significant number of defects and strains into the microstructure (48, 49).

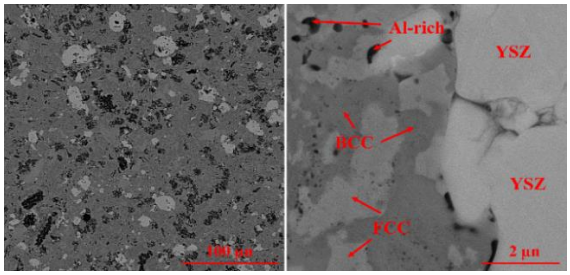

(a)

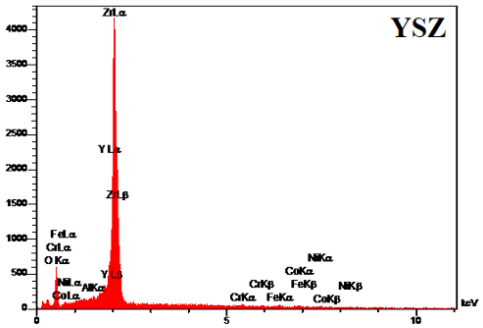

(b)

Figure 7. a) SEM image of the SPS-processed AlCoCrFeNi-10 wt. % YSZ, and, b) EDS analysis

TABLE 2. Results of EDS analysis taken from HEA, H5Y, and H10Y in different phases

	HEA		HEA-5YSZ			HEA-10YSZ		
	FCC	**BCC**	**FCC**	**BCC**	**YSZ**	**FCC**	**BCC**	**YSZ**
Al	4.57	19.81	3.85	16.13	---	4.58	20.12	---
Co	26.56	21.48	24.53	21.59	---	25.29	22.69	---
Cr	23.43	11.58	24.42	11.78	---	25.51	8.14	---
Fe	26.76	17.03	29.49	16.95	---	28.50	16.04	---
Ni	18.68	30.11	17.71	33.55	---	16.11	33.01	---
O	---	---	---	---	27.18	---	---	29.46
Zr	---	---	---	----	67.74	---	---	60.81
Y	---	---	---	---	5.09	---	---	9.73

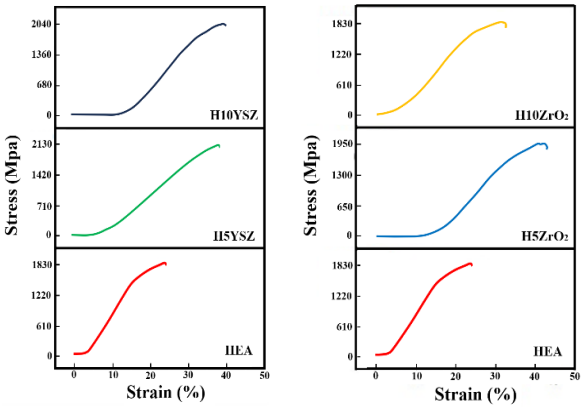

(a) (b)

Figure 8. Compressive engineering stress-strain curves of a) HEA-x wt.% YSZ and, b) ZrO_2 (X=0, 5, and 10)

TABLE 3. Mechanical properties of AlCoCrFeNi + x wt.% YSZ and ZrO_2 (x =0, 5, and 10)

Specimens	ε_p (%)	σ_y (MPa)	σ_{max} (MPa)
HEA	10	1520	1830
HEA-5YSZ	9	1760	2130
HEA-5ZrO_2	8	1650	1830
HEA-10YSZ	8	1680	2040
HEA-10ZrO_2	7.5	1550	1950

The SEM fractography inspection of the fracture surfaces of the HEA specimen is presented in Figure 9(a). The fracture surface of the unreinforced HEA specimen exhibits dimple features, indicating that this sample undergoes both elastic and plastic deformation during the compression tests. Therefore, the fracture mechanism identified for this AlCoCrFeNi high entropy alloy is characterized by cleavage fracture and slip separation. The fracture surface of the HEA-5 wt.% YSZ specimens is illustrated in Figure 9(b). It is observed that the dimples on the fracture surface of this specimen have become shallower which correlates with a reduction in ductility for this sample. The fracture surface images of the HEA-10 wt.% YSZ specimen in Figure 9(c) show that the number of dimples has decreased dramatically, indicating a brittle fracture mode. Still, the features of ductile fracture exist.

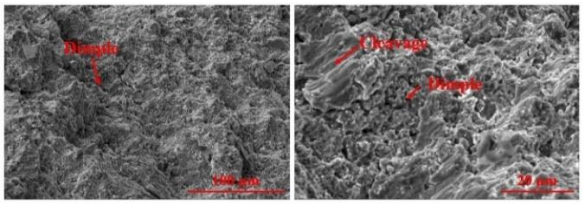

(a)

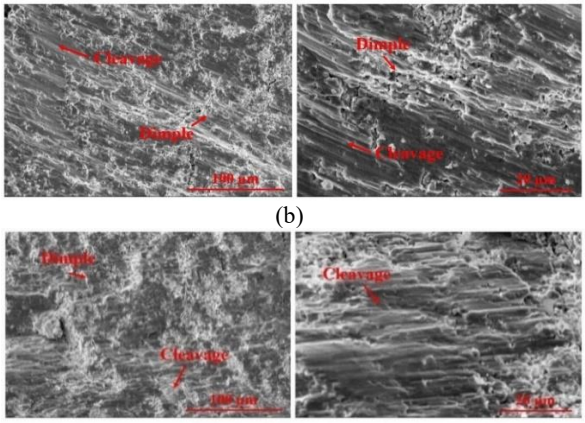

(b)

(c)

Figure 9. Fracture surfaces of a) HEA, b) HEA-5 wt.% YSZ, and c) HEA-10 wt.% YSZ specimens after compression test at room temperature

Figure 10 illustrates the fracture surface of H5Z and H10Z specimens. The figures show that HEA matrix specimens reinforced with ZrO_2 have several dimples on their fracture surface, indicating a localized ductile fracture. The observed cellular fracture surfaces in this figure are similar to those in Figure 9.

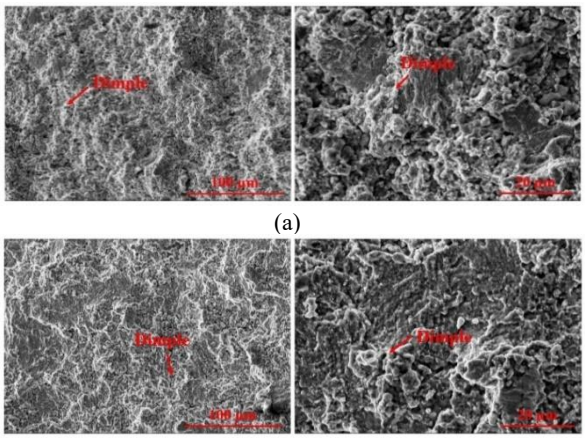

(a)

(b)

Figure 10. Fracture surfaces a) HEA-5 wt.% ZrO_2 and, b) HEA-10 wt.% ZrO_2

4. CONCLUSION

This research involved the preparation of AlCoCrFeNi + x wt.% YSZ and ZrO_2 (with x = 0, 5, and 10) specimens using mechanical alloying and SPS methods. Following the mechanical alloying of the elemental powders for 30 hours, a single-phase HEA powder with a BCC crystal structure was achieved. The sintering process of the HEA powder resulted in the formation of both BCC and FCC

phases, which can be attributed to the rapid heating rate associated with the SPS process and the limited time available for the complete transformation from BCC to FCC. By the increment of ceramic particles percentage, the phase fraction of FCC remained almost constant but the amount of BCC phase decreased. Due to better CTE compatibility, HEA-YSZ composites consist of a lower amount of Al-rich phase and more BCC phase compared to HEA-ZrO_2 composites. The results of compression tests showed that the addition of ceramic particulates enhanced the strength of the HEA matrix. This improvement is more pronounced in the specimens with 5 wt.% reinforcement. While σ_y in the unreinforced specimen is 1550 MPa, in the H5Y specimen, the yield strength increased to 1760 MPa. In contrast, the H10Y specimen exhibited a drop in yield strength attributed to a lower percentage of the BCC phase (36 wt.%) present in this sample. Similarly, the H5Z specimen, with 39% wt. BCC phase, achieved a yield strength of 1650 MPa, while the H10Z specimen had a reduced percentage of BCC phase (31 wt.%) and lower yield strength (1550 MPa). The observed behavior can be correlated to the phase structure of the specimens. The analysis of the fracture surfaces confirmed the coexistence of both brittle and ductile fracture modes after the compression tests.

Acknowledgements

The authors acknowledge Materials and Energy Research Center (MERC) for providing necessary facilities to conduct present research.

Funding

The authors declare that no financial support was received for this study.

Ethics Approval and Consent to Participate

This article does not involve any studies with human participants or animals performed by any of the authors. Therefore, ethics approval and consent to participate are not applicable.

Competing Interests

This article has no conflict with studies by other authors in this field.

Data Availability

All data generated or analyzed during this study are included in this published article.

Declaration of Generative AI and AI-assisted Technologies in the Writing Process

During the preparation of this manuscript, the authors used ChatGPT to improve the clarity of language and to correct grammar. The authors reviewed and edited the content as needed and take full responsibility for the content of the publication.

REFERENCES

1. Yeh JW, Chen SK, Lin SJ, Gan JY, Chin TS, Shun TT, et al. Nanostructured high-entropy alloys with multiple principal elements: novel alloy design concepts and outcomes. Advanced engineering materials. 2004;6(5):299-303. https://doi.org/10.1002/adem.200300567
2. Cantor B, Chang IT, Knight P, Vincent A. Microstructural development in equiatomic multicomponent alloys. Materials Science and Engineering: A. 2004;375:213-8. https://doi.org/10.1016/j.msea.2003.10.257
3. Chen J, Zhou X, Wang W, Liu B, Lv Y, Yang W, et al. A review on fundamental of high entropy alloys with promising high–temperature properties. Journal of Alloys and Compounds. 2018;760:15-30. https://doi.org/10.1016/j.jallcom.2018.05.067
4. Ye Y, Wang Q, Lu J, Liu C, Yang Y. High-entropy alloy: challenges and prospects. Materials Today. 2016;19(6):349-62. https://doi.org/10.1016/j.mattod.2015.11.026
5. Wang F, Zhang Y, Chen G, Davies H. Cooling rate and size effect on the microstructure and mechanical properties of AlCoCrFeNi high entropy alloy. 2009. https://doi.org/10.1115/1.3120387
6. Zhang Y, Zuo TT, Tang Z, Gao MC, Dahmen KA, Liaw PK, et al. Microstructures and properties of high-entropy alloys. Progress in materials science. 2014;61:1-93. https://doi.org/10.1016/j.pmatsci.2013.10.001
7. Chikumba S, Rao VV, editors. High entropy alloys: development and applications. Proceedings of the 7th International Conference on Latest Trends in Engineering & Technology (ICLTET'2015); 2015.
8. Miracle DB, Senkov ON. A critical review of high entropy alloys and related concepts. Acta materialia. 2017;122:448-511. https://doi.org/10.1016/j.actamat.2016.08.081
9. Ren B, Liu Z, Li D, Shi L, Cai B, Wang M. Effect of elemental interaction on microstructure of CuCrFeNiMn high entropy alloy system. Journal of Alloys and Compounds. 2010;493(1-2):148-53. https://doi.org/10.1016/j.jallcom.2009.12.183
10. Ji W, Fu Z, Wang W, Wang H, Zhang J, Wang Y, et al. Mechanical alloying synthesis and spark plasma sintering consolidation of CoCrFeNiAl high-entropy alloy. Journal of Alloys and Compounds. 2014;589:61-6. https://doi.org/10.1016/j.jallcom.2013.11.146
11. Zhang A, Han J, Meng J, Su B, Li P. Rapid preparation of AlCoCrFeNi high entropy alloy by spark plasma sintering from elemental powder mixture. Materials Letters. 2016;181:82-5. https://doi.org/10.1016/j.matlet.2016.06.014
12. Mohanty S, Maity T, Mukhopadhyay S, Sarkar S, Gurao N, Bhowmick S, et al. Powder metallurgical processing of equiatomic AlCoCrFeNi high entropy alloy: Microstructure and mechanical properties. Materials Science and Engineering: A. 2017;679:299-313. https://doi.org/10.1016/j.msea.2016.09.062
13. Ma Y, Jiang B, Li C, Wang Q, Dong C, Liaw PK, et al. The BCC/B2 morphologies in Al x NiCoFeCr high-entropy alloys. Metals. 2017;7(2):57. https://doi.org/10.3390/met7020057

14. Wang W-R, Wang W-L, Yeh J-W. Phases, microstructure and mechanical properties of AlxCoCrFeNi high-entropy alloys at elevated temperatures. Journal of Alloys and Compounds. 2014;589:143-52. https://doi.org/10.1016/j.jallcom.2013.11.084
15. Fu Z, Chen W, Wen H, Chen Z, Lavernia EJ. Effects of Co and sintering method on microstructure and mechanical behavior of a high-entropy Al0. 6NiFeCrCo alloy prepared by powder metallurgy. Journal of Alloys and Compounds. 2015;646:175-82. https://doi.org/10.1016/j.jallcom.2015.04.238
16. Chen Z, Chen W, Wu B, Cao X, Liu L, Fu Z. Effects of Co and Ti on microstructure and mechanical behavior of Al0. 75FeNiCrCo high entropy alloy prepared by mechanical alloying and spark plasma sintering. Materials Science and Engineering: A. 2015;648:217-24. https://doi.org/10.1016/j.msea.2015.08.056
17. Manzoni A, Daoud H, Völkl R, Glatzel U, Wanderka N. Phase separation in equiatomic AlCoCrFeNi high-entropy alloy. Ultramicroscopy. 2013;132:212-5. https://doi.org/10.1016/j.ultramic.2012.12.015
18. Wang F, Zhang Y. Effect of Co addition on crystal structure and mechanical properties of Ti0. 5CrFeNiAlCo high entropy alloy. Materials Science and Engineering: A. 2008;496(1-2):214-6. https://doi.org/10.1016/j.msea.2008.05.020
19. Lin C-M, Tsai H-L. Evolution of microstructure, hardness, and corrosion properties of high-entropy Al0. 5CoCrFeNi alloy. Intermetallics. 2011;19(3):288-94. https://doi.org/10.1016/j.intermet.2010.10.008
20. Ghanbariha M, Ketabchi M, Farvizi M. Investigation of alumina reinforcement effects on microstructure, hardness, and tribological behavior of AlCoCrFeNi high entropy alloy. Intermetallics. 2025;185:108915. https://doi.org/10.1016/j.intermet.2025.108915
21. Uporov S, Bykov V, Pryanichnikov S, Shubin A, Uporova N. Effect of synthesis route on structure and properties of AlCoCrFeNi high-entropy alloy. Intermetallics. 2017;83:1-8. https://doi.org/10.1016/j.intermet.2016.12.003
22. Han Z, Liang S, Yang J, Wei R, Zhang C. A superior combination of strength-ductility in CoCrFeNiMn high-entropy alloy induced by asymmetric rolling and subsequent annealing treatment. Materials Characterization. 2018;145:619-26. https://doi.org/10.1016/j.matchar.2018.09.029
23. Shahmir H, Nili-Ahmadabadi M, Shafiee A, Langdon TG. Effect of a minor titanium addition on the superplastic properties of a CoCrFeNiMn high-entropy alloy processed by high-pressure torsion. Materials Science and Engineering: A. 2018;718:468-76. https://doi.org/10.1016/j.msea.2018.02.002
24. Eleti R, Raju V, Veerasham M, Reddy S, Bhattacharjee P. Influence of strain on the formation of cold-rolling and grain growth textures of an equiatomic HfZrTiTaNb refractory high entropy alloy. Materials Characterization. 2018;136:286-92. https://doi.org/10.1016/j.matchar.2017.12.034
25. Han Z, Luan H, Liu X, Chen N, Li X, Shao Y, et al. Microstructures and mechanical properties of TixNbMoTaW refractory high-entropy alloys. Materials Science and Engineering: A. 2018;712:380-5. https://doi.org/10.1016/j.msea.2017.12.004
26. Senkov O, Wilks G, Miracle D, Chuang C, Liaw P. Refractory high-entropy alloys. Intermetallics. 2010;18(9):1758-65. https://doi.org/10.1016/j.intermet.2010.05.014
27. Rahmani M, Petrudi AM. Experimental and numerical optimization study of shock wave damping in aluminum panel sandwich. Fracture and Structural Integrity. 2021;15(55):88-109. https://doi.org/10.3221/IGF-ESIS.55.07
28. Saindane U, Soni S, Menghani J. Dry sliding behavior of carbon-based brake pad materials. International Journal of Engineering Transactions B: Applications. 2021;34(11):2517-24. https://doi.org/10.5829/ije.2021.34.11b.14
29. Saindane U, Soni S, Menghani J. Friction and wear performance of brake Pad and optimization of manufacturing parameters using grey relational analysis. International Journal of Engineering, Transactions C: Aspects. 2022;35:552-9. https://doi.org/10.5829/ije.2022.35.03c.07
30. Saindane U, Soni S, Menghani J. Performance evaluation of brake pads developed using two different manufacturing methods. Materialwissenschaft und Werkstofftechnik. 2023;54(2):186-95. https://doi.org/10.1002/mawe.202100407
31. Jha P, Gupta P, Kumar D, Parkash O. Synthesis and characterization of Fe–ZrO2 metal matrix composites. Journal of Composite Materials. 2014;48(17):2107-15. https://doi.org/10.1177/0021998313494915
32. Ding J, Zhao N, Shi C, Du X, Li J. In situ formation of Cu–ZrO2 composites by chemical routes. Journal of alloys and compounds. 2006;425(1-2):390-4. ttps://doi.org/10.1016/j.jallcom.2006.01.058
33. Yu H, Hou Z, Guo X, Chen Y, Li J, Luo L, et al. Finite element analysis on flexural strength of Al2O3-ZrO2 composite ceramics with different proportions. Materials Science and Engineering: A. 2018;738:213-8. https://doi.org/10.1016/j.msea.2018.05.075
34. Hemanth J. Development and property evaluation of aluminum alloy reinforced with nano-ZrO2 metal matrix composites (NMMCs). Materials Science and Engineering: A. 2009;507(1-2):110-3. https://doi.org/10.1016/j.msea.2008.11.039
35. Grigor'eva T, Letsko A, Talako T, Tsybulya S, Vorsina I, Barinova A, et al. Producing Cu/ZrO2 composites by combining mechanical activation and self-propagating high-temperature synthesis. Combustion, Explosion, and Shock Waves. 2011;47(2):174-8. https://doi.org/10.1134/S0010508211020055
36. Chang C, Wang Y, Pei H, Lee C, Du X, Huang J. Microstructure and mechanical properties of nano-ZrO2 and nano-SiO2 particulate reinforced AZ31-Mg based composites fabricated by friction stir processing. Key Engineering Materials. 2007;351:114-9. https://doi.org/10.4028/www.scientific.net/KEM.351.114
37. Shackelford JF, Doremus RH. Ceramic and glass materials. JF Shackelford, RH Doremus. 2008:28-329.
38. Srivastava M, Srinivasan A, Grips VW. Influence of zirconia incorporation on the mechanical and chemical properties of Ni-Co alloys. American Journal of material science. 2011;1(2):113-22.
39. Ghanbariha M, Farvizi M, Ebadzadeh T. Microstructural development in nanostructured AlCoCrFeNi–ZrO2 high-entropy alloy composite prepared with mechanical alloying and spark plasma sintering methods. Materials Research Express. 2019;6(12):1265b5. https://doi.org/10.1088/2053-1591/ab5fc9
40. Ghanbariha M, Farvizi M, Ebadzadeh T, Samiyan AA. Effect of ZrO2 particles on the nanomechanical properties and wear behavior of AlCoCrFeNi–ZrO2 high entropy alloy composites. Wear. 2021;484:204032. https://doi.org/10.1016/j.wear.2021.204032
41. Zhou P, Xiao D, Yuan T. Microstructure, mechanical and corrosion properties of AlCoCrFeNi high-entropy alloy prepared by spark plasma sintering. 金属学报英文版. 2020;33(7):937-46. https://doi.org/10.1007/s40195-019-00962-8
42. Farvizi M, Ebadzadeh T, Vaezi M, Yoon E, Kim Y, Kim H, et al. Microstructural characterization of HIP consolidated NiTi–nano Al2O3 composites. Journal of Alloys and Compounds. 2014;606:21-6. https://doi.org/10.1016/j.jallcom.2014.03.184
43. George EP, Raabe D, Ritchie RO. High-entropy alloys. Nature reviews materials. 2019;4(8):515-34. https://doi.org/10.1038/s41578-019-0121-4
44. Farvizi M, Bahamirian M, Faraji A, Kim H. Influence of ceramic reinforcement characteristics on the microstructure and wear

behavior of NiTi matrix composites. Materialia. 2023;28:101726. https://doi.org/10.1016/j.mtla.2023.101726

45. Mirazimi J, Abachi P, Purazrang K. Spark plasma sintering of ultrafine YSZ reinforced Cu matrix functionally graded composite. Acta Metallurgica Sinica (English Letters). 2016;29(12):1169-76. https://doi.org/10.1007/s40195-016-0512-0
46. Baba NB, Davidson A, Muneer T. YSZ-reinforced Ni-P deposit: An effective condition for high particle incorporation and porosity level. Advanced Materials Research. 2011;214:412-7. https://doi.org/10.4028/www.scientific.net/AMR.214.412
47. Wang YS, Tan MJ, Chua BW, Bayraktar E. YSZ-Reinforced Mg-Based amorphous composites: processing, characterisation & corrosion. Advanced Materials Research. 2014;939:122-9. https://doi.org/10.4028/www.scientific.net/AMR.939.122
48. Yim D, Sathiyamoorthi P, Hong S-J, Kim HS. Fabrication and mechanical properties of TiC reinforced CoCrFeMnNi high-entropy alloy composite by water atomization and spark plasma sintering. Journal of Alloys and Compounds. 2019;781:389-96. https://doi.org/10.1016/j.jallcom.2018.12.119
49. Jiao W, Li T, Chang X, Lu Y, Yin G, Cao Z, et al. A novel Co-free Al0. 75CrFeNi eutectic high entropy alloy with superior mechanical properties. Journal of Alloys and Compounds. 2022;902:163814. https://doi.org/10.1016/j.jallcom.2022.163814

Persian Abstract

چکیده

در این مطالعه، کامپوزیت‌های آلیاژ با آنتروپی بالا (HEA) متشکل از زمینه AlCoCrFeNi و تقویت‌کننده‌های مبتنی بر زیرکونیا، با استفاده از روش‌های آلیاژی مکانیکی (MA) و تف جوشی پلاسمای جرقه‌ای (SPS) ایجاد شدند. تجزیه و تحلیل ریزساختاری، وجود هر دو فاز FCC و BCC را پس از ۳۰ ساعت آلیاژسازی مکانیکی و سپس SPS در دمای ۱۰۰۰ درجه سانتیگراد نشان داد. همچنین، پالایش ریتولد نشان داد که درصد وزنی فاز FCC در هر دو کامپوزیت HEA و HEA-YSZ تقریباً یکسان بوده و افزودن ذرات YSZ منجر به کاهش فاز BCC گردید و در عین حال رشد دانه فازهای HEA را در طول زمان تفجوشی محدود نمود. نتایج آزمایش فشار نشان داد که در نمونه حاوی ۵ درصد وزنی YSZ به دلیل توزیع مناسب و درصد بالاتر فاز BCC (٤٠٪)، مقادیر استحکام تسلیم به ۱۷٦۰ مگاپاسکال افزایش یافت، در حالی که در نمونه با ۱۰ درصد وزنی YSZ، استحکام تسلیم به دلیل درصد کمتر فاز BCC (۳٦٪) کاهش یافت. یافته‌های این تحقیق نشان می‌دهد که کامپوزیت‌های AlCoCrFeNi تقویت‌شده با YSZ نسبت به کامپوزیت هایی که با ذرات ZrO_2 تقویت شده‌اند، در ترکیب مشابه استحکام تسلیم بیشتری نشان می‌دهند که به نسبت بالاتر فاز BCC در کامپوزیت‌های تقویت‌شده با YSZ و خواص ذاتی بهتر این تقویت کننده نسبت داده می‌شود. بررسی مکانیسم‌های شکست، نشانگر ترکیب شکست نرم و ترد در نمونه‌ها است.